Flexural properties and impact behaviour analysis of bamboo cellulosic fibers filled cement based composites

Xiaoli Xie [a,*], Zuowan Zhou [b], Yun Yan [a]

[a] School of Materials Science and Engineering, Southwest University of Science and Technology, Mianyang 621010, PR China
[b] Key Laboratory of Advanced Technologies of Materials (Ministry of Education), School of Materials Science and Engineering, Southwest Jiaotong University, Chengdu 610031, PR China

HIGHLIGHTS

- Bamboo cellulosic fibers increase remarkably fracture toughness of composites.
- Bamboo cellulosic fibers improve significantly impact resistance of composites.
- Impact resistance increases with the increase of fibers within certain content.
- There is a good correlation between impact energy and failure patterns.
- The values of the energy absorption can reflect the impact resistance of materials.

ARTICLE INFO

ABSTRACT

The flexural properties and impact resistance of the composites with bamboo cellulosic fiber (BF) weight fractions ranging from 4% to 16% was investigated using a universal testing machine and a full instrumented drop weight impact system, respectively. The effect of addition of BF on the flexural properties and impact resistance of the composites was estimated according to max flexural strength, fracture toughness, the contact force, failure pattern and absorbed energy. On the basis of the above results, the impact behaviour of the specimens with 12 wt% BF was examined from the point of view of the impact energy change, the deformation feedback and the absorbed energy. Additionally, impact damage morphology and extent were analyzed using the digital camera and an industrial microfocus computed tomography (CT) system. The results show that BF reinforced cement based composites have higher fracture toughness and impact energy absorbility, the fracture toughness and absorbed energy of the specimens with 4–16 wt% BF are higher by 2.7–45.9 times and 2–24 times than that of the control specimen, respectively. However, due to fibers agglomeration resulted from fibers addition beyond certain content, max flexural strength and impact resistant of the composites no further increase. Furthermore, the different impact energy leads to the different failure patterns and energy absorption modes: at low impact energy, the main energy absorption modes are the debonding between fiber and the matrix; with the increase of the impact energy, the main energy absorption modes are delamination and BF breakage.

© 2019 Elsevier Ltd. All rights reserved.

1. Introduction

In recent years, utilization of natural fibers in cement based composites has attracted increasing attentions, due to their many advantages over traditional fibers, such as biodegradability, economical and eco-friendly, etc. [1–5]. And natural fibers have already been considered as potential alternatives to traditional fibers (steel fiber, polymer fibers, glass fiber) [6]. Many studies in previous references have reported the influence of natural fibers on the properties of cement based composites, such as flexural properties [7–9], crack resistance [10,11], durability [12–14] and impact resistance [15–17], and the results show addition of the natural fibers can remarkably improve the toughness of the cementitious materials.

Generally, the capacity of absorption energy of the composites is defined as "toughness", which is very important for evaluating the service behavior of composite materials under actual conditions when fibers reinforced composites are subjected to static, dynamic or fatigue loading [15]. It is well known that the impact

test is a method to evaluate the toughness and ductility of cement based materials [18], while the impact strength is a specific parameter to measure the toughness of materials under dynamic impact loading. Therefore, the impact test is necessary for studying the toughness of fibers reinforced cement based composites, because it is convenient to understand and evaluate the behavior and characteristics of fibers reinforced cement based composites in a variety of potential uses.

Previous investigations on fibers reinforced cement based composites have paved a strong foundation in understanding the impact behavior of cement based composites filled fibers and the results have shown that the addition of the randomly oriented fibers can improved remarkably the impact resistance of concrete [15–22]. Ramakrishna and Sundararajan [15] investigated the impact strength of four natural fibers (including coir, sisal, jute and hibiscus cannebinus) reinforced cement mortar slabs under a repeated projectile test. The impact resistant of the cement mortar slabs reinforced with fibers were 4–19 times of the cement mortar slabs without fibers. Zhou et al. [17] studied the effect of addition of jute fiber on mortar panels under a repeated drop hammer test, and found that addition of jute fiber result in much higher impact resistant than the mortar panels without jute fiber. Mohammadi et al. [19] observed the impact resistant of steel fiber reinforced concrete by means of drop weight test. They evaluated the impact resistant of the specimens by blows number of the impact hammer when the first crack and ultimate failure produced in the specimens. According to the previous research, for evaluating the impact resistance, the repeated impact (drop weight) test was the simple technique and usually used. Additionally, two kinds of criterion, including energy required for specimen cracking and the number of strikes required to reach a certain cracking level, are used to determine the impact resistance of the specimens [15,23]. However, the above method cannot measure the instantaneous state of the composite in the impact process. Moreover, the comprehensive reports about the impact behaviour of natural fibers/cement based composites have not been found in the previous literatures.

Combined the above discussions with the static bending test, the main purpose of this paper is to investigate the flexural properties and the impact behavior of the composites with 4, 8, 12 and 16 wt% BF content. And then, on the basis of the above experimental results, the specimens with 12 wt% BF were fabricated, and the impact test was carried out under the five different impact energy (5, 10, 15, 20 and 25 J). In addition, impact damage morphology and extent were analyzed by means of the digital camera and an industrial microfocus computed tomography (CT) system. The relationship among the contact force, the absorbed energy, the deformation and the damage state of the specimens under the different impact energy are examined, further the impact damage mechanisms of BF reinforced cement based composites are analyzed and assessed.

2. Materials and methods

2.1. Raw materials and specimens preparation

Bamboo cellulosic fiber (BF), with an average length and standard deviation of 2.5 ± 0.4 mm and an average diameter and standard deviation of 13.1 ± 4.6 μm, was obtained from Sichuan Anxian Paper Co., Ltd. of China. The chemical composition of the BF comprehends approximately 92.0% α-cellulose, 2.5% hemicellulose, 0.2% lignin and 1.4% ash. SEM images of BF were shown in Fig. 1.

42.5 ordinary Portland cement (OPC) was sourced from China United Cement Corporation. The chemical composition of OPC (Table 1) were determined by X-ray fluorescence, and the particle size distribution (Fig. 2) of OPC were measured by laser granulometry.
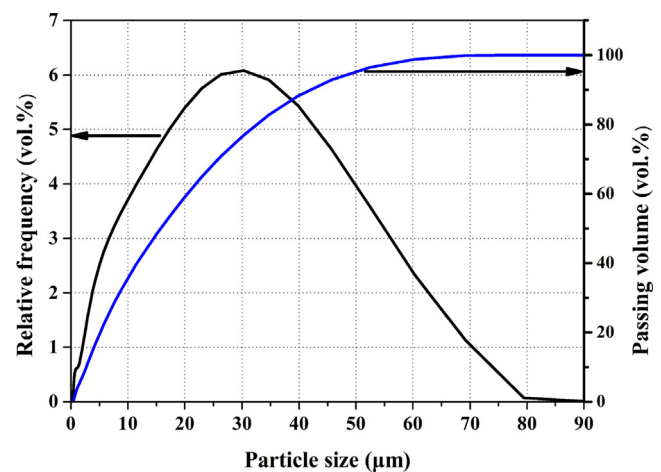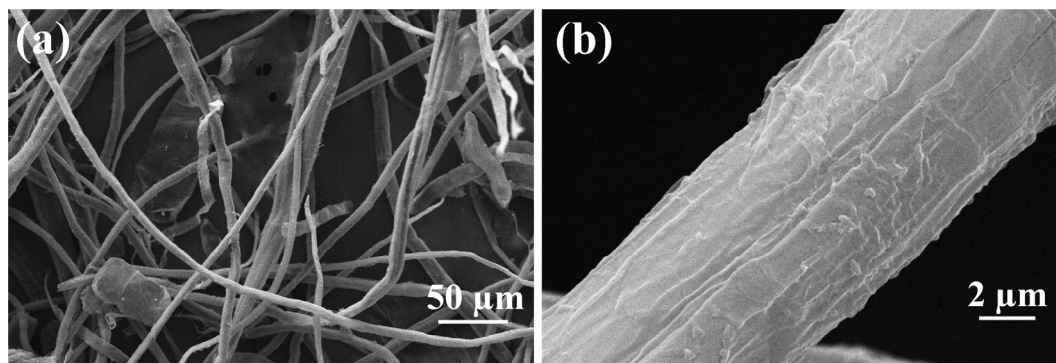

Fig. 2. Particle size distribution of OPC.

Fig. 1. SEM images of bamboo cellulosic fibers (BF).

Table 1
The chemical composition of OPC/wt.%

Components	Al$_2$O$_3$	CaO	Fe$_2$O$_3$	K$_2$O	MgO	Na$_2$O	P$_2$O$_5$	SO$_3$	SiO$_2$	TiO$_2$	BaO
OPC	4.83	62.4	2.85	0.81	2.39	0.41	0.35	4.73	18.9	0.47	0.14

In this study, the cement based composites reinforced with 4, 8, 12 and 16 wt% (% of fiber by weight of solid components) BF were investigated, and pure cement paste as control specimen. The composite slabs were prepared using a slurry vacuum de-watering technique, as described in the authors' previous work [24]. BF were stirred by the household Soybean milk maker for 2.5 min before OPC was added, then the slurry was stirred at 1500 rpm in the planetary mixer for an additional 2.5 min. Solids was 10–20% of the slurry according to the different BF content. Later, the slurry was quickly transferred to the casting box, excessive water was sucked by vacuum (approximately 80 kPa gauge) and then the specimens were pressed at 3.2 MPa for 5 min. All demoulded test specimens were firstly sealed in the plastic bag for one day at room temperature, and then cured in the temperature of $(20 \pm 1)\,°C$ and relative humidity exceeding 90% until 28 days. For each mixture series, the circular plate specimens having 130 mm in diameter and 10 mm in thickness were prepared for the impact test. Furthermore, the $160\,mm \times 40\,mm \times 8\,mm$ rectangle specimens were prepared for the physical properties measurement and bending test. For the impact test three specimens were prepared for each mix design, for the physical properties (water absorption, apparent porosity and bulk density) and the bending test six specimens were used.

2.2. Test and analysis

In this study, the bending test were performed using the WSM-10kN universal testing machine by the three-point bending tests, whose displacement control rate and span were 0.5 mm/min and 100 mm, respectively. In the process of the bending test, the load-deflection curves of each mixture series were obtained according to the testing machine record. Max flexural strength and fracture toughness were calculated as Eqs. (1) and (2).

$$\text{Max flexural strength} = 3PL/2bd^2 \tag{1}$$

$$\text{Fracture toughness} = \text{Fracture energy}/bd \tag{2}$$

where max flexural strength represents the max flexural strength in MPa, P represent the maximum load (in N) recorded in the testing, l represents span of support specimen, b represents specimen breadth, and d represents specimen depth. The fracture energy (in Joules) is measured by enveloped area of load-deflection curve to the point corresponding to a reduction in the load carrying capacity to 50% of the maximum load observed, as described in Ref. [24–26].

After the bending test, the fracture surface of the specimens were conducted by TM-4000 scanning electron microscope (SEM) at 15.0 kV accelerating voltage. In addition, the physical properties of the specimens were calculated according to ASTM C 948-81 test method.

An Instron CEAST 9350 drop hammer machine (as shown in Fig. 3) equipped with automatic anti-rebound systems was used to measure the impact behaviour of the specimens. All impact tests were carried out using a hemispherical hammer, whose diameter and mass were 20 mm and 5.5 kg, respectively. Moreover, the shape and mass of the hammer was constant in all the tests. The data acquisition system of machine can obtain the instantaneous velocity, displacement and kinetic energy when the impact hammer head got in contact with the specimen. The impact test first was performed on the specimens with 4, 8, 12 and 16 wt% BF and the control specimen under the impact energy of 25 J. And then, combined the above experimental results with bending test results, the impact test of the specimens filled with 12 wt% BF was carried out under the five different impact energy (5, 10 15, 20 and 25 J). The record time of each test is 12 ms, and the impact hammer impact in the center of the specimens.

Fig. 3. CEAST 9350 impact test machine.

In the process of impact testing, the maximum contact force, maximum deformation and absorbed energy are deemed to three important parameters to assess impact behavior of the composites [27]. The value of impact energy is not only determined by the mass and falling height of the hammer head, but also related to the loss of energy in the free falling of the hammer head [28]. If the frictional force of the hammer is not been taken into account in the free fall, the impact energy is expressed as follows:

$$E_i = mgh = \frac{1}{2}mv^2 = E_a + E_b \tag{3}$$

where E_i is the impact energy (in Joules), m and h are the mass and the drop height of the hammer head, respectively, v is the impact velocity at which the hammer starts contact with the specimen; E_a is the absorbed energy by the specimens, which produces on the one hand a permanent deformation of the specimens, and on the other hand the dissipation of specimen damage, and E_b is the energy which remained in the system after the impact test was finished, including the frictional dissipated energy and the energy transmitted through the specimen to the instrument. The absorbed energy E_a is calculated by the enveloped area of contact force-deformation curves.

In some research [28–30], the Absorption Coefficient β, obtained by the absorbed energy E_a and impact energy E_i, was used to measure the characteristics of the specimens, defined as follows:

$$\beta = \frac{E_a}{E_i} \tag{4}$$

After impact testing, the impact damage morphology of the specimens was observed by using the digital camera to analyze the failure pattern and damage characterizations. In addition, the damage detection of the microstructure of the specimens was performed on an industrial microfocus computed tomography (CT) system (Germany Y.CT Precision).

3. Results and discussion

3.1. Effect of bamboo cellulosic fiber content

3.1.1. Physical properties analysis

Table 2 shows the physical parameter of the cement based composites filled different BF content. The results show that the addition of 4–16 wt% BF decreases the density of the composite specimens to 64.7–87.6% of that of the control specimen, and increases the water absorption and apparent porosity of the composite specimens to 1.4–2.0 times and 1.2–1.4 times of that of the control specimen, respectively. Besides, the higher the BF content, the lower the density, the higher the apparent porosity and water absorption. At the same time, in the case of the less BF content, the increase of 4 wt% BF content results in the more obvious changes of density, water absorption and apparent porosity. Corresponding to the control specimen without BF, the bulk density, water absorption and apparent porosity of the composites filled with 4 wt% BF change by 14.9%, 26.5% and 35.3%, respectively. Compared to BF content change from 0 to 4 wt%, the BF content change between 12 wt% and 16 wt% leads to the smaller change of the bulk density (4.4%), water absorption (4.6%) and apparent porosity (2.5%) of the composites.

3.1.2. Bending test analysis

Fig. 4 shows load-deflection curves from three-point bending test of the specimens with the different BF content. Figs. 5 and 6 show Max flexural strength, fracture toughness and SEM images of fracture surface of the specimens with the different BF content, respectively. It can be seen from Fig. 4 that the load-deflection curve of the control specimen is almost linear up to a peak point where an abrupt crack growth takes place with a sudden drop in load, indicating that the static fracture of the specimen without BF is brittle. However, the load-deflection curve of the composites filled with BF displays an initial linearity and subsequent nonlinear characteristic, and the decrease in load after passing the peak load is slow, indicating that the static fracture of the specimens with BF is ductile. In addition, the deflection value of the specimens in the load-deflection curves increase with the increase of BF content. The deflection value of the specimens at failure are about 3.5, 10.5, 19.0 and 22.0 times of that of the control specimen without BF when the BF content are 4, 8, 12 and 16 wt%. Based on the displacement load rate of 0.5 mm/min in the bending test, the test process of the specimens with 0, 4, 8, 12 and 16 wt% BF lasts about 0.8, 3.0, 7.4, 17.4 and 19.5 min, respectively.

Likewise, it can be seen from Fig. 5 that the fracture toughness value of the specimens increased by 2.7, 14.0, 34.1 and 45.9 times compared with the control specimen. The improvement of the BF addition on the fracture toughness can be attributed to interfacial interaction of fiber and matrix, as well as the absorbed energy when the fibers pulled out from cement matrix in the bending test. Consequently, within 16 wt% BF content, the more BF content the higher the deflection and fracture toughness of the specimens. However, the influence trend of BF content on max flexural strength is distinct from that of the deflection and fracture toughness. Firstly, max flexural strength value of the specimens reduces to 76.6% of that of the specimen without BF when BF content is 4 wt%. Morteza and Eshmaiel [7] studied the flexural behavior of
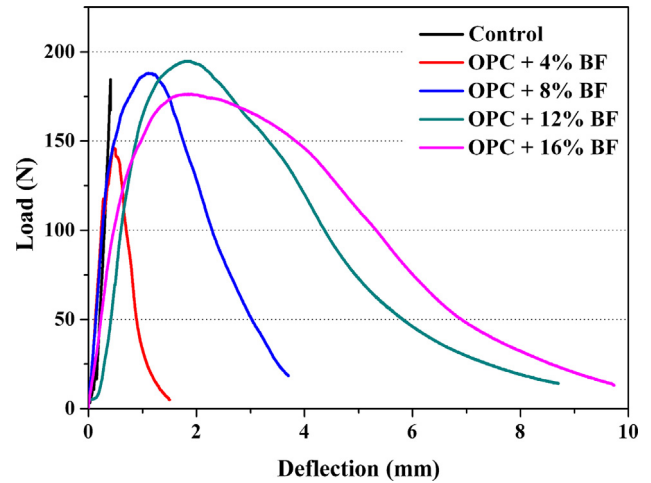

Fig. 4. Load-deflection curves of the specimens with the different BF content.
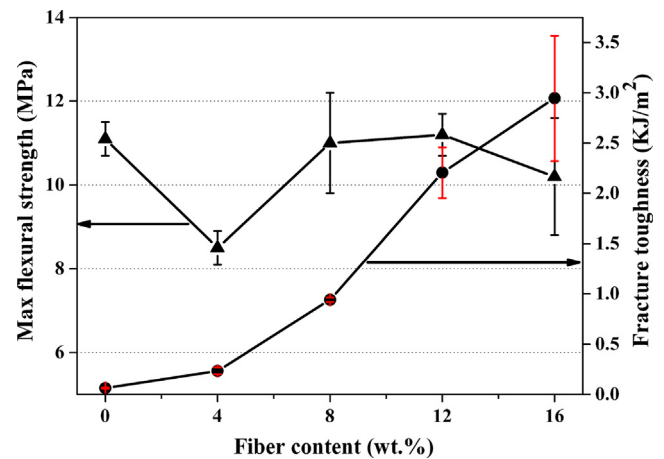

Fig. 5. Max flexural strength and fracture toughness of the specimens with the different BF content.

the fiber-cement composites reinforced several plant fiber, and deemed that a small amount fiber content was not enough to distribute uniformly in the cement matrix, as shown Fig. 6a. Therefore, cracks occur firstly in areas where fibers are not present, leading to specimen failure under less load. Then undergo a significant increase within 8–12 wt% BF content. Finally, adding of 16 wt% BF lead to about 8.9% in reducing max flexural strength value compared with the specimen with 12 wt% BF. The decrease of the max flexural strength can be ascribed to fiber agglomeration (Fig. 6d) induced by the high fiber content as discussed in Ref. [31].

In a word, according to the above analysis results, the flexural properties of the composite specimen is optimal when BF content is 12 wt%.

3.1.3. Impact behaviour analysis

The contact force-time curves of the specimens with four different BF content and the control specimen are shown in Fig. 7. The

Table 2
Physical parameters of bamboo cellulosic filled cement based composites.

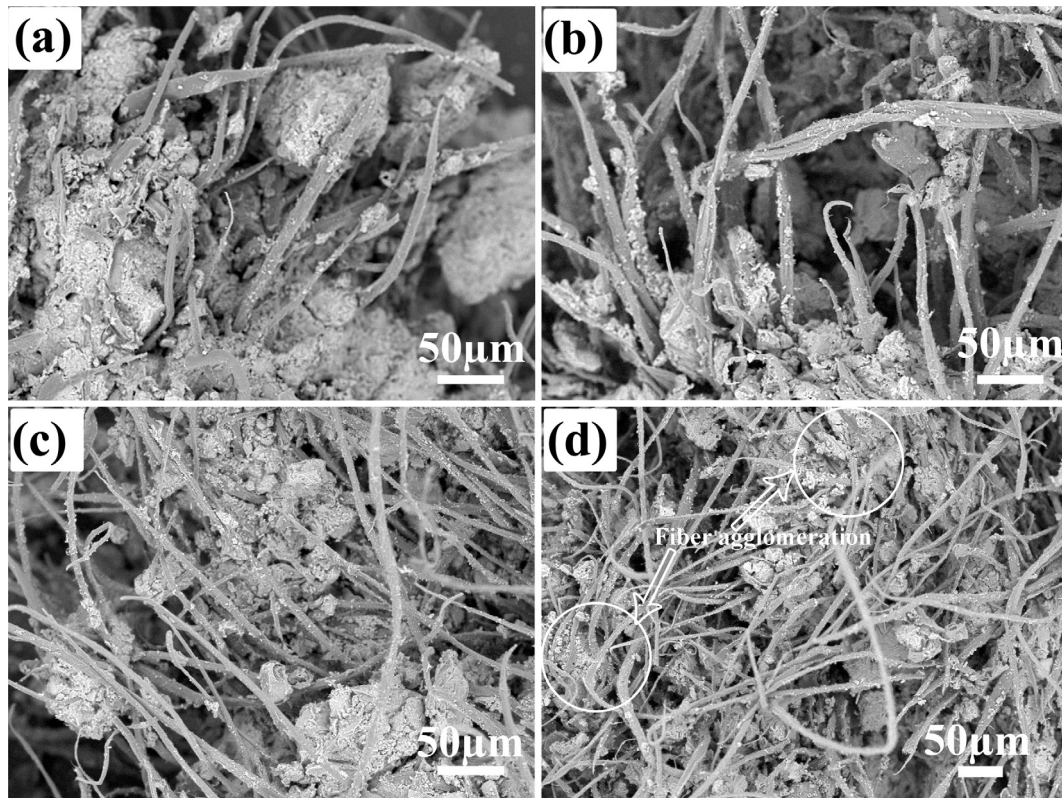| BF content (wt.%)	0	4	8	12	16
Bulk density (g/cm³)	2.01 ± 0.04	1.71 ± 0.01	1.50 ± 0.04	1.36 ± 0.04	1.30 ± 0.05
Water absorption (%)	13.6 ± 1.2	18.5 ± 0.5	21.2 ± 0.9	26.3 ± 1.4	27.5 ± 2.8
Apparent porosity (%)	26.8 ± 1.7	31.4 ± 1.0	32.2 ± 0.9	35.7 ± 1.2	36.6 ± 2.3

Fig. 6. SEM images of fracture surface of the specimens with the different BF content: (a) 4 wt% BF, (b) 8 wt% BF, (c) 12 wt% BF, (d) 16 wt% BF.

corresponding failure pattern of the different specimens are presented in Fig. 8 after impact testing. As seen in Figs. 7 and 8, the maximum contact force increases with increasing fiber content under the impact energy of 25 J, and addition of BF and variation of BF content result in the obvious change of contact force-time curves and failure pattern of the specimens. From Fig. 7a–c, it can be observed that the contact force-time curve of the control specimen is similar to those of the specimens with 4 and 8 wt% BF. The contact force firstly exhibit a sharp increase to a peak value, and then undergo a quickly decrease to a constant value of 0 N, later occurring drastic vibration centered the value of 0 N. Initial injury contact force is equal to peak contact force. It is indicated that the initial damage is the main damage in the impact test, which result in the serious damage and fracture of the slabs. As shown in Fig. 8a, 8b and 8c, the control specimen and the specimens with 4 and 8 wt% BF broken into pieces. And the amount of fragment and crack length decrease with the increase of BF content: the control specimen without BF broken into 6 pieces or more pieces, the specimens with 4 wt% BF broken into 4 pieces, while the specimens broken into 3 pieces when BF content is 8 wt%. Whereas, compared with Fig. 7a–c, the contact force of Fig. 7d and e increases linearly to a peak value accompanying with slight fluctuation at the very beginning of strike, and then reveals a significant decline. The peak contact force corresponds to the initial damage of the specimens. Afterwards the contact force rises and falls repeatedly, corresponding to the development of damage or the formation of new injury. Finally, the contact force decline continuously due to rebound of the drop weight at a certain speed, until the contact force decreases to zero, implying the complete separation of the specimen slab and the hammer head [19]. However, the initial damage contact force and peak contact force are different, indicating that the damage of the specimens is a gradual process. Manifest in the failure pattern of Fig. 8d–g, the specimens

with 12 and 16 wt% BF still remained the initial morphology, though the circular specimens also was subjected to slightly damaged. A pit was found on the top surfaces of the specimens contacted with the hammer (Fig. 8d and f). While bottom surfaces of the specimens cracked in many place (Fig. 8e and g), and the damaged areas was larger than that of the top surfaces. Additionally, the contact force-time curve and failure pattern of the specimens with 12 and 16 wt% BF almost was consistent.

In addition, comparing with the contact force-time curves of the different specimens in Fig. 7f, violent fluctuations was occurred in the control specimen and the composite specimen with 4 wt% BF after the contact force decrease to zero. Whereas the degree of fluctuations getting slighter and slighter with the increase of BF content, the fluctuations are almost negligible in the specimens with 12 and 16 wt% BF. As suggested by Wang et al. [32], the fluctuation of contact force implied the continuous breakage and cracking of fiber/cement composites. Therefore, within 12 wt% BF content, the impact resistance is linearly dependent with BF content, and the more serious the damage is, the greater the degree of the fluctuations becomes. In other words, addition of BF improves significantly the impact resistance of the specimens, because the bridging effect of the interlaminar fibers may significantly improve the cohesiveness and homogeneity of cement paste [33].

Furthermore, by comparing the contact force-time curves of Fig. 7f with the load-deflection curves of Fig. 4, it can be found that the test failure in the dynamic impact test is much shorter than the failure time in static bending test. As already mentioned, in the bending test, the test process of the specimens with 0, 4, 8, 12 and 16 wt% BF lasts about 0.8, 3.0, 7.4, 17.4 and 19.5 min, respectively. While the test failure in the impact test occurs within a few milliseconds (Fig. 7f). Moreover, the load-deflection curves of Fig. 4 indicates the maximum flexural load in the bending test is far lower than the maximum contact force in the impact test
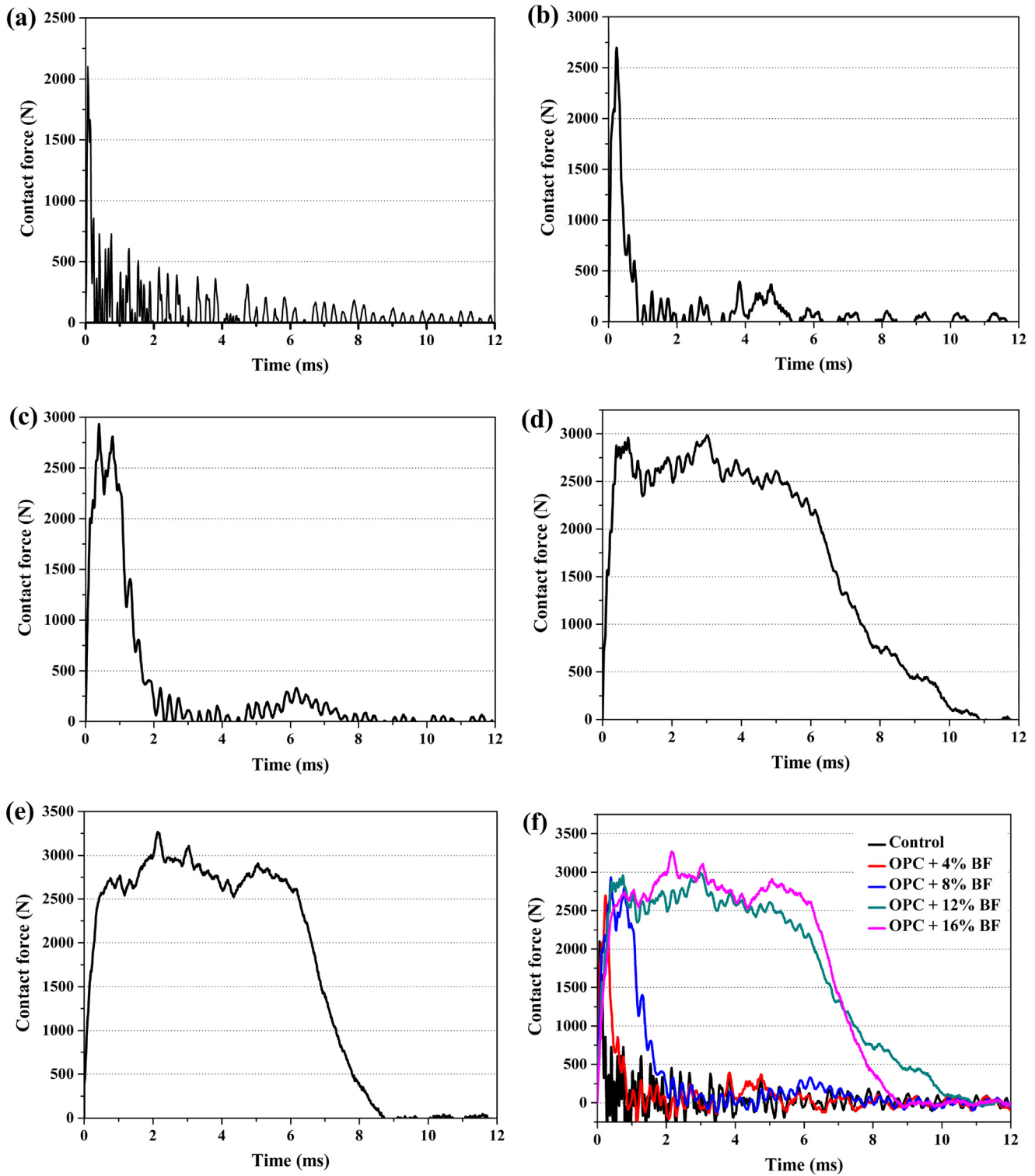
Fig. 7. Contact force-time curves: (a) control specimen, (b) 4 wt% BF, (c) 8 wt% BF, (d) 12 wt% BF, (e) 16 wt% BF, (f) the comparison of different specimens.

(Fig. 7f). For the bending test, the maximum load value is about 140–200 N, while the maximum contact force value in the impact test can be obtained 2700–3400 N. The above behavioral differences is related to the difference of the loading speed in the two kinds of tests. In general, when the external force acts quickly on the specimen, the plastic part is fixed while the elastic part shows significant performance, resulting in the higher failure stress value. If the dynamic impact test is regarded as a static test conducted at

a loading speed far greater than 0.5 mm/min, then its dynamic load value is far greater than that of the static one, which also conforms to the conclusion that the static strength trend increases with the acceleration of loading speed.

Contact force-deformation curves of the specimens with the different BF content are given in Fig. 9. The contact force-deformation curves of the specimens with 0, 4 and 8 wt% BF are similar to the contact force-time curves of Fig. 7. However, the curves of the
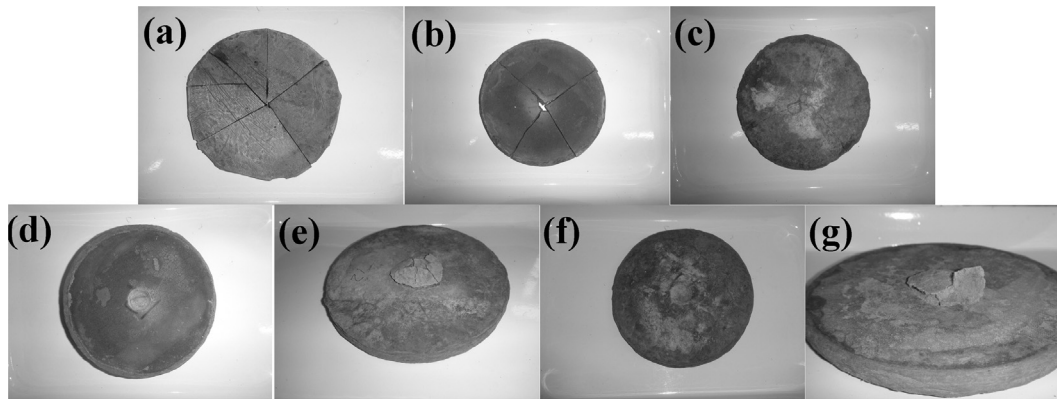
Fig. 8. The failure patterns of the specimens with the different BF content: (a) 0 wt% BF, (b) 4 wt% BF, (c) 8 wt% BF, (d) top surface of 12 wt% BF, (e) bottom surface of 12 wt%, (f) top surface of 16 wt% BF, (g) bottom surface of 16 wt%.

specimens with 12 and 16 wt% BF (Fig. 9d and 9e) have the obvious difference with the curves of Fig. 9a–c. The distinction attributed to the failure pattern of the specimens: fracture of the composite slabs was observed when BF content was 0, 4 and 8 wt%, while the curves of the composite slabs with 12 and 16 wt% BF obtained from the tests were rebounding case.

Table 3 presents absorbed energy E_a and the Absorption Coefficient β of the specimens filled with the different BF content, it can be seen that the composite slabs with BF absorbed much more energy than the control specimen under the same impact energy of 25 J. As shown in Table 3, the absorbed energy and the Absorption Coefficient significantly increase with the increase of BF content. As compared to 0.95 J of the control specimen, the absorbed energy of the specimens with 4, 8, 12 and 16 wt% BF increases to 2.71, 6.28, 23.16 and 23.51 J, respectively. Due to addition of 4–16 wt% BF, the absorbed energy is increased to 3–25 times of that of the control specimen. As a result, it seems that the more BF content leads to the higher energy absorption capacity. However, beyond 12 wt% BF, fiber agglomeration causes the formation of the "fiber ball", whose negative effect produced in the composites eliminate the positive effect of addition of fiber [31]. Xu et al. [20] proposed the absorbed energy of fiber reinforced cement based composites subjected to impact mainly depends on the matrix crack, the fiber/matrix debonding as well as fiber sliding. Moreover, the combination of the above three factors achieve the optimum state when the fiber weight fraction reaches a certain amount [34].

Overall, the effect of BF content is highly significant in both the static bending test and the dynamic impact test. In combination with the bending test results and the impact test behaviour, the bending properties and impact resistance of the composites achieve the optimal when BF content is 12 wt%.

3.2. Effect of impact energy

3.2.1. Impact damage parameters

Figs. 10 and 11 shows the contact force-time curves and contact force-deformation curves of the specimens with 12 wt% BF under the different impact energy, respectively. As shown in the figures, the maximum deformation of the specimens, contact time between the impact hammer head and the specimens generally increase with the increasing impact energy. In addition, at the beginning of the impact test, the contact force increases rapidly from zero to a peak force, this causes the violent fluctuation of the specimen and the hammer, as well as rapid change of the contact area between the specimen and the hammer head. The phenomenon reflected in the contact force–time curve is the

fluctuation of the contact force, which is consistent with the description of the previous Ref. [32]. Another reason for the fluctuation of the contact force is the continuous damage and cracking of the specimens. When the contact force fluctuates, the specimen and the hammer head keep in contact with each other and move downwards together until the contact force reaches the maximum. Subsequently, the hammer head and the specimen rebound together. However, the rebound speed of the hammer head is faster than the rebound speed of the specimen, leading to a decrease of contact area and a decline of contact force. Finally, the contact force drops to zero because the specimen and hammer are completely separated, as shown in Fig. 11. Therefore, the relevant study summarize the impact process into three stages, including vibrate stage, stable stage and unloading stage [24,35,36].

As described by Schoeppnera and Abrateb [37], in the stage of complete elasticity or minor damage, the peak contact force is affected by the impact energy and has a positive correlation with the depth of the pit, but there will be inflection point at certain contact force. In addition, other studies [38,39] indicate that initial damage contact force and peak contact force of the specimen is close under the different impact energy, showing a plateau shape. With respect to the certain specimen with certain thickness and supporting condition, the maximum contact force is a threshold value. When the impact energy increases and greater contact force is needed, "stress release" resulted from the damage of the specimen bring the maximum force back to the threshold value. The initial damage contact force and peak contact force appear increasing inflection point when the impact energy is 20 J, which illustrate the impact energy of 20 J is the damage threshold of the composite specimen with 12 wt% BF.

After being subjected to impact testing, the absorbed energy E_a and the Absorption Coefficient β of the specimens with 12 wt% BF are given in Table 4. As shown in the table, the absorbed energy increases with the increasing impact energy. When the impact energy is 5, 10, 15, 20 and 25 J, the corresponding absorbed energy E_a of the specimens are 3.82, 9.19, 14.35, 19.30 and 23.16 J, respectively. While the Absorption Coefficient β exhibit increase firstly and then decrease when the impact energy increase from 5 to 25 J. when the impact energy is 5, 10, 15, 20 and 25 J, the corresponding β are 0.76, 0.92, 0.96, 0.97 and 0.93, respectively. The above phenomena are consistent with the description in the Ref. [28]. When the different impact energy is applied to the same samples, lower impact energy result in less damage to the sample. Within the impact energy of 5 to 20 J, the permanent deformation of the specimens and the dissipation energy of specimen damage increase with the increase of impact energy, so the Absorption Coefficient β also increase with the increase of the impact energy.
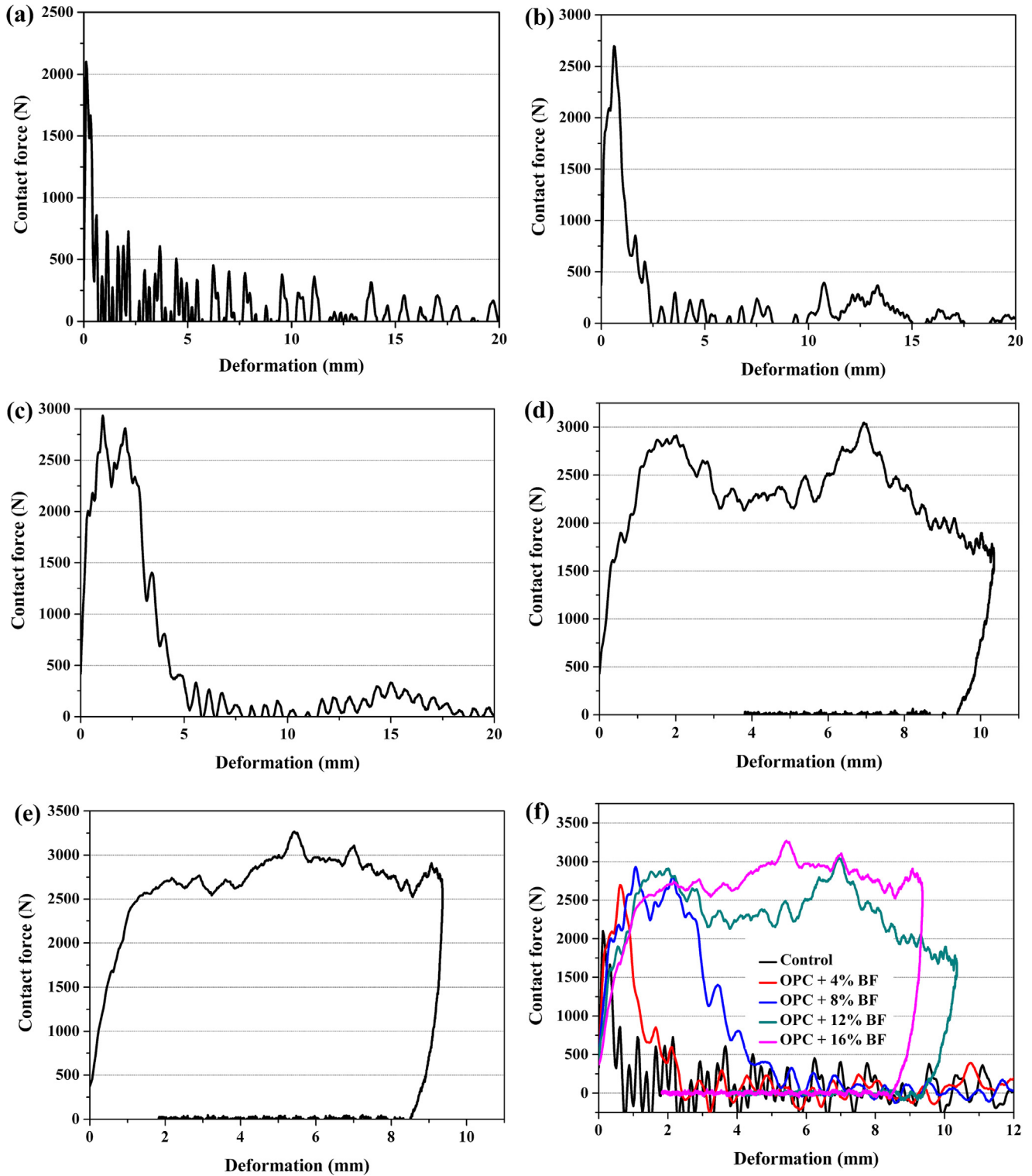
Fig. 9. Contact force-deformation curves: (a) control specimen, (b) 4 wt% BF, (c) 8 wt% BF, (d) 12 wt% BF, (e) 16 wt% BF, (f) the comparison of different specimens.

Table 3
E_a and β of the different specimens under the impact energy of 25 J.

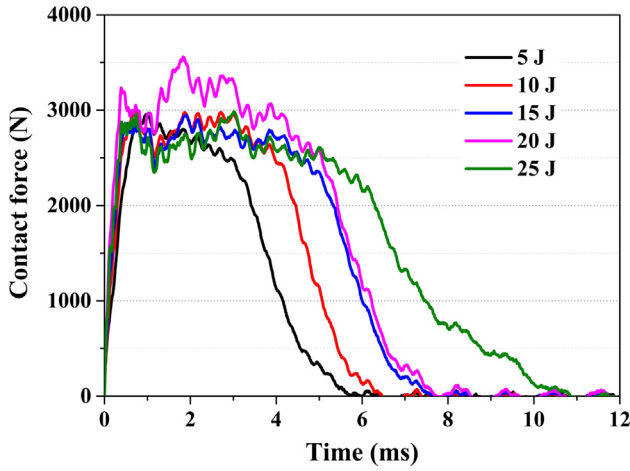| BF content (wt%)		0	4	8	12	16
Absorbed energy/E_a (J)	Average value	0.95	2.71	6.28	23.16	23.51
	Standard deviation	0.03	0.18	0.24	0.62	0.53
β		0.04	0.11	0.25	0.93	0.95

Fig. 10. Contact force-time curves of the specimens with 12 wt% BF under different impact energy.
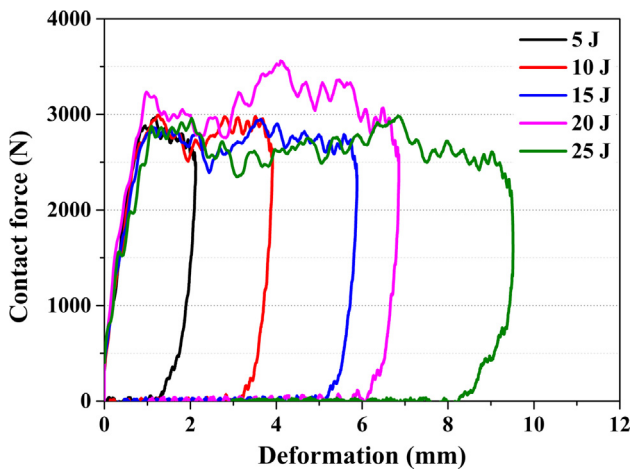

Fig. 11. Contact force-deformation curves of specimens with 12 wt% BF under different impact energy.

However, when the impact energy achieves a certain value, the increase of impact energy lead to the increasing damage degree of composite specimens, as well as the contact time between the specimens and the hammer head (Fig. 11). In this case, the energy E_b, including the frictional dissipated energy and the energy transmitted through the specimen to the instrument, also increase. Therefore, as the impact energy increases gradually, the value of E_a/E_i gradually increase to a certain inflection point and then decrease.

3.2.2. Failure pattern analysis

Figs. 12 and 13 present the two-dimension CT maps and three-dimension reconstruction figures in impact zone of the composite slabs after the impact test of the different impact energy (5, 10, 15 and 20 J), respectively. From Figs. 12 and 13, it is observed that the pits of different sizes were formed on top surfaces of the slabs,
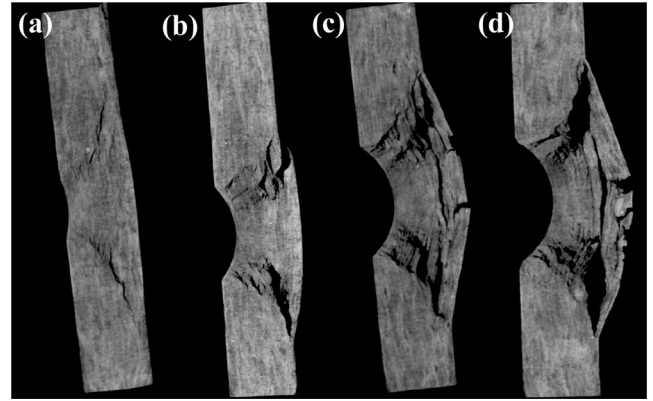

Fig. 12. The two-dimension CT maps of the specimens after impact test: (a) 5 J, (b) 10 J, (c) 15 J, (d) 20 J.

moreover, the depth of the pits increases with the increase of impact energy. Comparing with the damage on top surfaces of slabs, the damage shape on bottom surfaces of slabs is approximately circular, and the damage area is large than that of top surfaces. Additionally, the damage area and the amount of the matrix crack increase with the increasing impact energy. According to Fig. 12a and Fig. 13a, at the impact energy of 5 J, it is observed that there are matrix cracks, delamination and a small amount of fibers breakage in the inner of specimens. In addition, the delamination of the composite slabs is mainly perpendicular to the impact direction of the hammer head, and the cracking direction is along the sides of the cone, whose top and bottom surfaces correspond to the damage areas on top and bottom surfaces of the specimens. With the increase of impact energy, the impact loading transmit to the adjacent layer by the cement matrix and the interlocking point between fibers, resulting in both the more serious delamination and more cracks. Thus the delamination area and the number of cracks in the specimens are more than the damage on the surfaces of the specimens.

The above phenomenon could be explained by Fig. 14, in which Fig. 14a shows the state before the impact testing. In the case of low impact energy, the impact between the impact hammer head and the slabs generates the compressive stress waves, which are perpendicular to the surfaces of the specimens. After that, the compressive stress waves, propagating to the bottom surfaces of the specimens through the thickness of the specimens, are reflected back as the tensile stress waves [40,41], resulting in delamination in the specimens along the edge of the cone. And the direction of delamination is perpendicular to the impact direction of the hammer, as shown in Fig. 14b. In the case of increasing impact energy, delamination in the composite slabs occurs as the interlaminar stress induced by the tensile stress waves exceeds to the interlaminar strength. At the same time, in the process of formation of the reflected tensile stress waves, the interlaminar stress induced by the flexural stress wave lead to the continues expanding of delamination. Therefore, as shown in Fig. 14c, the radial delamination in the specimens further propagates from the edge to the interior of the cone [42]. According to opinion of interlaminar fracture, initial delamination will propagate when local interlaminar stress

Table 4
E_a and β of the composites reinforced with 12 wt% BF at different impact energy.

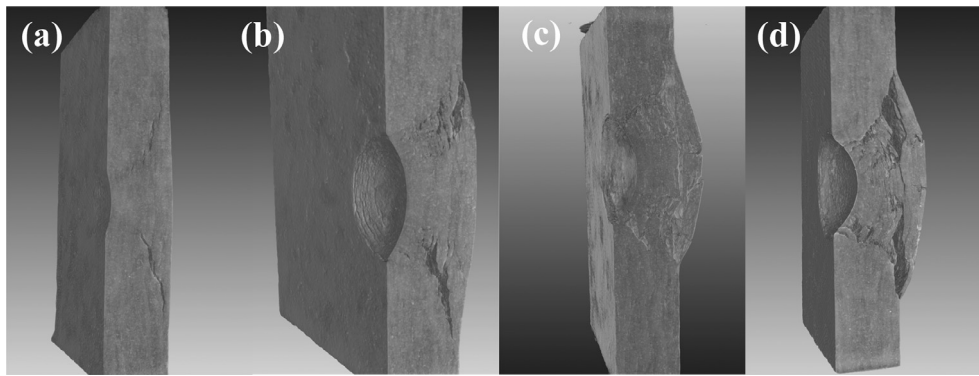| Impact energy (J)		5	10	15	20	25
Absorbed energy/E_a (J)	Average	3.82	9.19	14.35	19.30	**23.16**
	Standard deviation	0.09	0.30	0.13	0.36	**0.62**
β		0.76	0.92	0.96	0.97	**0.93**

Fig. 13. The three-dimension reconstruction figures of the specimens after impact test: (a) 5 J, (b) 10 J, (c) 15 J, (d) 20 J.
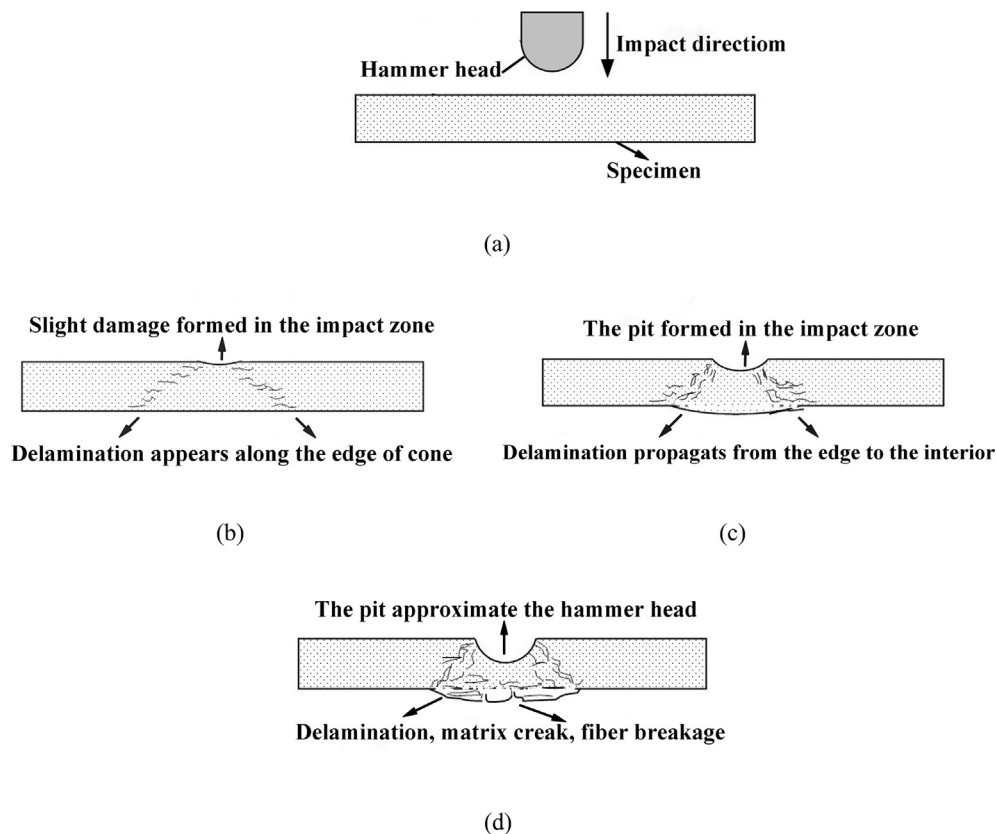

Fig. 14. The failure patterns of BF filled cement based composites under different impact energy.

produced by local bending makes the strain energy release rate G of stratified edge reach or exceed the critical value Gc (interlaminar fracture toughness), and then delamination will stop extending and form the final delamination damage until $G < G_c$ [43]. The continuous increasing impact energy brings about the more serious delamination in the specimens, where the matrix and fiber breakage appear the bottom surfaces or the interior of the specimens, which is the critical state of penetration damage (Fig. 14d).

Therefore, in the impact testing process of BF reinforced cement based composites, the specimens would delaminate in the perpendicular direction of the impact hammer head falling under low impact energy. At this moment, the specimens absorb energy by the means of debonding and delamination between BF and the matrix. With the increase of impact energy, the more serious damages, including delamination, matrix cracking, and a small quantity of BF brakeage, are observed in parallel to the impact direction of

the hammer head. At this moment, the specimens absorb energy by the means of debonding and delamination between BF and the matrix, as well as BF breakage. Based on the experimental results and the above discussion, BF reinforced cement based composites have the different failure patterns and energy absorption modes under the different impact energy. In addition, the two major energy absorption mechanisms involve delamination and BF breakage, as discussed in the previous study [29,44,45].

4. Conclusions

In this study, the bamboo cellulosic fibers were used as reinforcement of cementitious materials. The three point bending test was executed to evaluated the flexural properties of cement based composites with the different BF content (4, 8, 12 and 16 wt%). The

drop hammer impact test was operated to assess the effect of BF content and impact energy on the impact behaviour of the specimens. Furthermore, the failure pattern of bamboo cellulosic fibers reinforced cement based composites under different impact energy was developed. The following conclusion can be summarised from this study:

- Generally, the flexural properties of the specimens were improved remarkably due to the addition of 4–16 wt% BF. The maximum deflection and fracture toughness of the composites increase to 3.5–22.0 times and 3.7–46.9 times of the control specimen, respectively. However, the max flexural strength exhibit first decrease, then increase and again drop with the increase of BF content.
- As a reinforcement, addition of BF can improve significantly the impact resistance of cementitious materials. Within 12 wt% BF content, the impact resistance of BF reinforced cement based composites increases with the increase of the fibers content.
- Under the impact energy of 25 J, when the BF content is 4–16 wt %, the absorbed energy of the specimens are 3–25 times of that of the control specimen. While the specimens with 12 and 16 wt% BF obtained the almost same absorbed energy with the values of 23.16 and 23.51 J, respectively. Additionally, the smaller the absorbed energy value of the specimens is, the worse the impact resistance of the corresponding materials become.
- In term of the impact test of the specimens with 12 wt% BF, the different impact energy leads to the different failure patterns and energy absorption modes. At low impact energy, the composites delaminate in the perpendicular direction of the impact hammer falling, and the main energy absorption modes are the debonding between fiber and the matrix. With the increase of the impact energy, delamination is accompanied with the matrix cracks and fibers breakage, and the main energy absorption modes are delamination and BF breakage.
- Although addition of bamboo cellulosic fibers improve remarkably the flexural properties and impact behaviour of cement based composite, it is also important to assess the capacity of energy absorption after aging. So the team is studying long-term properties of bamboo cellulosic fiber filled cement based composites, and the corresponding results will be published later.

Conflict of Interest Statement

The authors declared that they have no conflicts of interest to this work.

Acknowledgements

Appendix A. Supplementary data

Supplementary data to this article can be found online at https://doi.org/10.1016/j.conbuildmat.2019.06.029.

References

[1] P. Soroushian, J.P. Won, M. Hassan, Durability characteristics of CO_2-cured cellulose fiber reinforced cement composites, Constr. Build. Mater. 34 (2012) 44–53.
[2] Ö. Andiç-Çakir, M. Sarikanat, H.B. Tüfekçi, C. Demirci, Ü.H. Erdoğan, Physical and mechanical properties of randomly oriented coir fiber-cementitious composites, Compos. Part B – Eng. 61 (2014) 49–54.
[3] R.D.T. Filho, F.D.A. Silva, E.M.R. Fairbairn, J.D.A.M. Filho, Durability of compression molded sisal fiber reinforced mortar laminates, Constr. Build. Mater. 23 (2009) 2409–2420.
[4] G.H.D. Tonoli, U.P. Rodrigues, H. Savastano Jr, J. Bras, M.N. Belgacem, F.A.R. Lahr, Cellulose modified fibres in cement based composites, Compos. Part A – Appl. Sci. 40 (2009) 2046–2053.
[5] F. Pacheco-Torgal, S. Jalali, Cementitious building materials reinforced with vegetable fibres: A review, Constr. Build. Mater. 25 (2011) 575–581.
[6] J.Q. Wei, C. Meyer, Degradation of natural fiber in ternary blended cement composites containing metakaolin and montmorillonite, Corros. Sci. 120 (2017) 42–60.
[7] M. Khorami, E. Ganjian, Comparing flexural behaviour of fibre-cement composites reinforced bagasse: wheat and eucalyptus, Constr. Build. Mater. 25 (2011) 3661–3667.
[8] H.J. Savastano, S.F. Santos, M. Radonjic, W.O. Soboyejo, Fracture and fatigue of natural fiber reinforced cementitious composites, Cem. Concr. Compos. 31 (2009) 232–243.
[9] A. Sellami, M. Merzoud, S. Amziane, Improvement of mechanical properties of green concrete by treatment of the vegetals fibers, Constr. Build. Mater. 47 (2013) 1117–1124.
[10] G.H.D. Tonoli, M.N. Belgacem, G. Siqueira, J. Bras, Savastano HJ. Rocco, FA., Processing and dimensional changes of cement based composites reinforced with surface-treated cellulose fibres, Cem. Concr. Compos. 37 (2013) 68–75.
[11] R.D.T. Filho, K. Ghavami, M.A. Sanjuán, G.L. England, Free, restrained and drying shrinkage of cement mortar composites reinforced with vegetable fibres, Cem. Concr. Compos. 27 (2005) 537–546.
[12] R.D.T. Filho, K. Scrivener, G. England, K. Ghavami, Durability of alkali-sensitive sisal and coconuts fibres in cement mortar composites, Cem. Concr. Compos. 22 (2000) 127–143.
[13] J.D.A.M. Filho, F.D.A. Silva, R.D.T. Filho, Degradation kinetics and aging mechanisms on sisal fiber cement composite systems, Cem. Concr. Compos. 40 (2013) 30–39.
[14] J.Q. Wei, C. Meyer, Degradation mechanisms of natural fiber in the matrix of cement composites, Cem. Concr. Res. 73 (2015) 1–16.
[15] G. Ramakrishna, T. Sundararajan, Impact strength of a few natural fibre reinforced cement mortar slabs: a comparative study, Cem. Concr. Compos. 27 (2005) 547–553.
[16] S.K. Al-Oraimi, A.C. Seibi, Mechanical characterization and impact behaviour of concrete reinforced with natural fibres, Compos. Struct. 32 (1995) 165–171.
[17] X.M. Zhou, S.H. Ghaffar, W. Dong, O. Oladiran, M. Fan, Fracture and impact properties of short discrete jute fibre-reinforced Ncementitious composites, Mater. Design 49 (2013) 35–47.
[18] A. Badr, A.F. Ashour, A.K. Platten, Statistical variations in impact resistance of polypropylene fiber-reinforced concrete, Int. J. Impact Eng. 32 (2006) 1907–1920.
[19] Y. Mohammadi, R. Carkon-Azad, S.P. Singh, S.K. Kaushik, Impact resistance of steel fibrous concrete containing fibres of mixed aspect ratio, Constr. Build. Mater. 23 (1) (2009) 183–189.
[20] B. Xu, H.A. Toutanji, J. Gilbert, Impact resistance of poly (vinyl alcohol) fiber reinforced high-performance organic aggregate cementitious material, Cem. Concr. Res. 40 (2010) 347–351.
[21] N. Mahmoud, V. Afroughsabet, The effects of silica fume and polypropylene fibers on the impact resistance and mechanical properties of concrete, Constr. Build. Mater. 24 (2010) 927–933.
[22] N. Banthia, C. Yan, K. Sakai, Impact resistance of fiber reinforced concrete at subnormal temperatures, Cem. Concr. Compos. 20 (1998) 393–404.
[23] P.N. Balaguru, S.P. Shah, Fibre-reinforced cement composites, McGraw Hill Inc, UK, 1992, p. 530.
[24] X.L. Xie, Z.W. Zhou, M. Jiang, X.L. Xu, Z.Y. Wang, D. Hui, Cellulosic fibers from rice straw and bamboo used as reinforcement of cement-based composites for remarkably improving mechanical properties, Compos. Part B – Eng. 78 (2015) 153–161.
[25] H. Savastano Jr, P.G. Warden, R.S.P. Coutts, Brazilian waste fibres as reinforcement for cement-based composites, Cem. Concr. Compos. 22 (2000) 379–384.
[26] N. Neithalath, Damage assessment in cellulose cement composites using dynamic mechanical characteristics, Cem. Concr. Compos. 28 (2006) 658–667.
[27] M.E. Deniz, R. Karakuzu, Seawater effect on impact behavior of glass-epoxy composite pipes, Compos. Part B – Eng. 43 (2012) 1130–1138.
[28] D. Zhu, M. Gencoglu, B. Mobasher, Low velocity flexural impact behavior of AR glass fabric reinforced cement composites, Cem. Concr. Compos. 31 (2009) 379–387.
[29] M. Quaresimin, M. Ricotta, L. Martello, S. Mian, Energy absorption in composite laminates under impact loading, Compos. Part B – Eng. 44 (2013) 133–140.
[30] E.D. Mehmet, O. Mustafa, O. Okan, K. Ramazan, M.I. Bulent, Environmental effect on fatigue life of glass-epoxy composite pipes subjected to impact loading, Compos. Part B – Eng. 44 (2013) 304–312.
[31] S. Chakraborty, S.P. Kundu, A. Roy, R.K. Basak, S.B. Adhikari, S.B. Majumder, Improvement of the mechanical properties of jute fibre reinforced cement mortar: A statistical approach, Constr. Build. Mater. 38 (2013) 776–784.
[32] Y.F. Wang, X.D. An, J.Y. Richard Liew, M.H. Zhang, Experimental behavior of cement filled pipe-in-pipe composite structures under transverse impact, Int. J. Impact Eng. 72 (2014) 1–16.

[33] S.S. Wang, H.T.N. Le, L.H. Poh, H.J. Feng, M.H. Zhang, Resistance of high-performance fiber-reinforced cement composites against high-velocity projectile impact, Int. J. Impact Eng. 95 (2016) 89–104.

[34] D. Sedana, C. Pagnoux, A. Smitha, T. Chotard, Mechanical properties of hemp fibre reinforced cement: Influence of the fibre/matrix interaction, J. Eur. Ceram. Soc. 28 (2008) 183–192.

[35] M. Yousuf, B. Uy, Z. Tao, A. Remennikov, J.Y.R. Liew, Transverse impact resistance of hollow and concrete filled stainless steel columns, J. Constr. Steel Res. 82 (2013) 177–189.

[36] A.M. Remennikov, S.Y. Kong, B. Uy, The response of foam- and concrete-filled square steel tubes under low-velocity impact loading, J. Perform Constr. Fac. 25 (5) (2011) 373–381.

[37] G.A. Schoeppnera, S. Abrateb, Delamination threshold loads for low velocity impact on composite laminates, Compos. Part A – Appl. Sci. 31 (2000) 903–915.

[38] P. Feraboli, K.T. Kedward, A new composite structure impact performance assessment program, Compos. Sci. Technol. 66 (2006) 1336–1347.

[39] G.A.O. Davies, P. Robinson, J. Robson, D. Eady, Shear driven delamination propagation in two dimensions, Compos. Part A – Appl. Sci. 28 (8) (1997) 757–765.

[40] K. Krishnann, S. Sockalingam, S. Bansal, et al., Numerical simulation of ceramic composite armor subjected to ballistic impact, Compos. Part B – Eng. 41 (2010) 583–593.

[41] E. Celal, G. Müfit, Effective damage mechanisms and performance evaluation of ceramic composite armors subjected to impact loading, J. Compos. Mater. 48 (26) (2014) 3215–3236.

[42] J.L. Puente, A. Arias, R. Zaera, et al., The effect of the thickness of the adhesive layer on the ballistic limit of ceramic/metal armors: an experimental and numerical study, Int. J. Impact Eng. 32 (2005) 321–336.

[43] J. Zhang, C. Soutis, J. Fan, Strain energy release rate associated with local delamination in cracked composite laminates, Composites 25 (1994) 851–862.

[44] W.J. Cantwell, J. Morton, Impact perforation of CFRP, Compos. Sci. Technol. 38 (1990) 119–141.

[45] W.J. Cantwell, J. Morton, The influence of varying projectile mass on the impact response of CFRP, Compos. Struct. 13 (1989) 101–114.